




MoPE: Parameter-Efficient and Scalable Multimodal Fusion via Mixture of Prompt Experts

Jiang Ruixiang¹, Lingbo Liu¹, and Changwen Chen¹

The Hong Kong Polytechnic University, Hong Kong SAR
rui-x.jiang@connect.polyu.hk
{lingbo.liu, changwen.chen}@polyu.edu.hk

Abstract. Prompt-tuning has demonstrated parameter-efficiency in fusing unimodal foundation models for multimodal tasks. However, its limited adaptivity and expressiveness lead to suboptimal performance when compared with other tuning methods. In this paper, we address this issue by disentangling the vanilla prompts to adaptively capture dataset-level and instance-level features. Building upon this disentanglement, we introduce the mixture of prompt experts (MoPE) technique to enhance expressiveness. MoPE leverages multimodal pairing priors to route the most effective prompt on a per-instance basis. Compared to vanilla prompting, our MoPE-based conditional prompting exhibits greater expressiveness for multimodal fusion, scaling better with the training data and the overall number of trainable parameters. We also study a regularization term for expert routing, leading to emergent expert specialization, where different experts focus on different concepts, enabling interpretable soft prompting. Extensive experiments across three multimodal datasets demonstrate that our method achieves state-of-the-art results, matching or even surpassing the performance of fine-tuning, while requiring only 0.8% of the trainable parameters. Code will be released: <https://github.com/songrise/MoPE>.

Keywords: Multimodal Fusion · Prompt Tuning · Mixture of Experts

1 Introduction

Empowered with billion-scale data and highly scalable model architectures, recent unimodal pre-trained models [3, 4, 17, 28, 35], also known as foundation models, have demonstrated their transferable power to various downstream tasks [26, 30, 51]. However, transferring multimodal foundation models for downstream applications is less flexible. Recent explorations, such as CLIP [34], employ two-tower designs that entangle the two encoders, meaning that replacing either one would necessitate expensive paired pre-training from scratch. This limitation hinders the broader application that would benefit from a specific unimodal architecture, such as longer context windows. To democratize foundation models, a

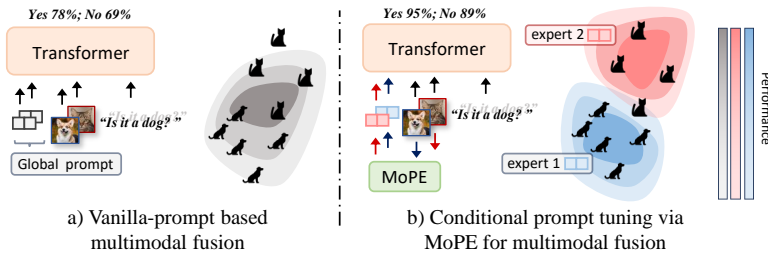


Fig. 1: High-level motivation of MoPE-based conditional prompting. a) vanilla prompt tuning learn a global shared prompt for all instances, which may not be optimal for each instance; b) MoPE-based conditional prompt tuning optimize multiple specialized prompt experts and is instance-wise adaptive.

compelling question arises: *How can we efficiently combine separately pretrained unimodal foundation models for downstream multimodal tasks?*

Recently, prompt tuning [11, 20] has emerged as a novel paradigm for parameter-efficient transfer learning. While originally proposed for low-shot adaptation to tasks with the same modality as they were pretrained on [11, 20, 50], it has also proven effective for multimodal fusion. Typically, this is achieved by abstracting the representation from one modality into one or a few prompts, which are fed into the frozen Transformer of another modality for fusion [21, 22, 39, 45].

Despite the effectiveness of prompt tuning in inter-modality transfer learning, directly adopting it for multimodal fusion could yield suboptimal results, particularly due to its limited adaptivity and scalability. Notably, while prompt tuning generally performs well in low-data regimes, it can be less effective when applied to full-shot training on the entire dataset with a challenging objective [7, 19, 22, 39, 44]. This reduced efficacy could be attributed to at least two factors. First, the vanilla prompt tuning used in previous prompt-based fusion methods [21, 22, 39] is not designed for multimodal tasks. These methods simply optimize a globally shared prompt for all instances [11, 20, 39], neglecting the multimodal interplay and potentially failing to capture the locally optimal representation for each input instance. Second, the relatively small number of trainable parameters (compared with fine-tuning) can lead to underfitting in multimodal datasets with a long-tail distribution and complex cross-modal mapping [27, 32, 42].

To address these challenges, increasing the number of learnable prompts, known as “*length-scaling*,” appears to be a plausible solution. Despite its apparent simplicity, a lot of research indicates that the performance gains from length-scaling quickly reach saturation in both unimodal [7, 19] and multimodal cases [22, 39, 44]. Furthermore, over-length prompts may even lead to worse results [11, 14, 16, 20, 44]. Recent theoretical analyses have substantiated these empirical observations, highlighting the limited expressiveness of prompt tuning [32, 42]. A direct implication of their analysis is that simply increasing prompt length is insufficient to address the issues of adaptivity and expressiveness.

Based on the above observations, we aim to enhance the expressiveness of the vanilla prompt used in multimodal fusion to improve adaptivity and scalability. Our motivation is to utilize the multimodal input pairing information as a prior, and to scale up the prompt in another dimension—the number of prompt experts—rather than length, as illustrated in Fig. 1. To accomplish this, we first propose a conditional prompt tuning method, which disentangles the vanilla global-shared prompt vector into static and dynamic prompts to adaptively capture global and local features. The cornerstone of our dynamic prompt generation is our innovative MoPE (**M**ixture of **P**rompt **E**xperts) design. In this design, we fix the prompt length used in attention and scale up expressiveness by learning multiple prompt experts and a router at each layer. We then use the representation from another modality as a prior to route the most effective dynamic prompt for each instance, enabling adaptive fusion.

We show that our MoPE-based fusion method alleviates the two issues in previous prompt-based fusion methods by allowing instance-wise adaptive prompting and avoiding over-length deterioration for better scalability. We systematically compare our MoPE-based fusion method with previous fusion methods on three multimodal datasets, UPMC Food-101 [41], SNLI-VE [43] and MM-IMDB [1]. Not only does our method deliver state-of-the-art results on all datasets, it also has higher parameter-efficiency compared with methods based on vanilla prompting, due to our improved adaptivity and expressiveness. Specifically, we achieve results comparable to fine-tuning while requiring only $\sim 0.8\%$ of the trainable parameters, and we outperform previous state-of-the-art (SOTA) prompt-based methods by a significant margin. Additionally, we demonstrate the superior scalability of our method. Our analysis indicates that increasing the number of experts (*i.e.* “*expert-scaling*”) tends to be a better alternative than length-scaling, which avoids performance deterioration with an overly-long prompt. In addition to parameter scaling, our method also demonstrates better scalability with increased training data. Finally, as the first endeavor to use prompts as experts, we analyze how different methods of expert routing can affect expert specialization. Thanks to the proposed regularization term, we observe the emergence of specialized prompt experts after end-to-end training, achieving high interpretability compared to black-box conditional prompting. We summarize our contributions as follows:

- We design a conditional prompt tuning method for multimodal fusion, which disentangles the vanilla prompt as static, dynamic and mapped prompts for better adaptiveness.
- We introduce the MoPE technique for instance-wise dynamic prompt generation, which scales up the expressiveness of prompt tuning for multimodal fusion.
- A combination of regularization terms is studied to aid expert specialization.
- Extensive experiments on UPMC Food-101, SNLI-VE and MM-IMDB datasets demonstrate state-of-the-art performance and parameter-efficiency for multimodal fusion.

2 Related Works

Prompt Tuning for Transfer Learning. Prompt tuning involves learning continuous token embedding as additional input to a frozen pretrained model for transfer learning. This technique was first popularized in NLP [19, 20], then quickly introduced to CV society [2, 11, 23, 25] and multimodal learning [12, 14, 47, 49]. For either modality, researchers empirically report good transfer learning performance in low-shot adaptation, yet its performance is less comparable to fine-tuning when abundant training instances are available [7, 20]. Moreover, increasing prompt length quickly reaches performance saturation, and over-length prompts might have a negative impact on performance [11, 16, 44]. Recent theoretical analysis [32, 42] reveal that the expressiveness of vanilla prompt tuning is lower than fine-tuning and LoRA [10]. In this work, we scale up the expressiveness of vanilla prompting by employing a Mixture of Experts (MoE)-like design.

Multimodal Fusion via Prompt. Apart from adapting models, prompts can also be used to fuse separately pretrained *unimodal models* for multimodal tasks. This is a **different** task from the commonly known “multimodal prompt tuning”, which usually refers to using prompts for transfer learning of multimodal pretrained foundation models. Frozen [39] first introduces a method where the visual representation is mapped as a few input tokens to query frozen language models (LM). PromptFuse and BlindPrompt [22] improved upon this by introducing tunable prompts to the LM for cross-model alignment. PICa [45] translate images into discrete text captions to prompt frozen LMs. These methods treat tokens from different modalities independently and lack cross-modal interaction. Recently, PMF [21] introduced an interactive prompt-tuning method, but their interactivity is built on the strong assumption that both encoders are white-box and in the same Transformer architecture. In this work, we further investigate how to efficiently utilize cross-modal features for prompting while maintaining high modularity by treating one modality as a black box.

MoE in Transformers. MoE is a powerful technique to scale up models, including Transformers [6, 18, 31, 36]. The fundamental approach involves inserting MoE layers, composed of multiple feed-forward networks (FFNs) acting as experts, into the standard Transformer architecture. A router is learned to route each token embedding to the most suitable expert(s). Due to the significant computational cost associated with FFN forwarding, a sparse gating function is typically employed to limit the number of experts used per token [33, 36, 38]. Thanks to those designs, the MoE layer can efficiently scale up model capacity while maintaining computational efficiency. Inspired by previous FFN-based MoE, we explore scaling up the vanilla prompting with an MoE design.

3 Method

Our objective is to adaptively and efficiently fuse unimodal pretrained models for solving multimodal tasks via prompt tuning. In this section, we first review the

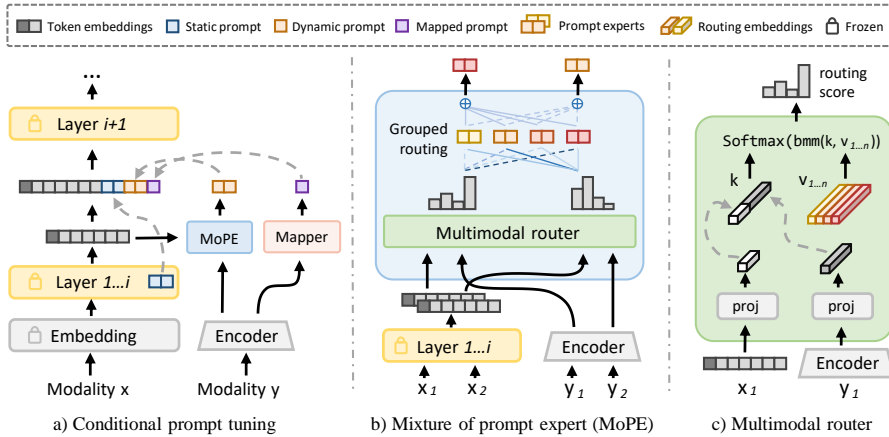


Fig. 2: Architecture overview. We illustrate the proposed MoPE-based multimodal fusion method when applied to one frozen Transformer layer. a) We sequentially fuse two modalities, using modality y to guide the prompting of modality x through a three-type prompt disentanglement process. (b) MoPE is introduced, utilizing the multimodal pairing as a prior to instance-wisely generate the dynamic prompt; (c) Inside the multimodal router, we project the representation from each modalities. The concatenated feature (along channel dimension) is used to match the routing embedding paired with each experts for routing score calculation. Better viewed with color.

working mechanism and the limitation of vanilla prompt tuning in Sec. 3.1. In Sec. 3.2, we explain how we achieve conditional prompt-tuning via a sequential pipeline and disentangled prompt tuning. In Sec. 3.3 we introduce the proposed MoPE, consisting of multiple prompt experts and a multimodal router for expressiveness scaling. Finally, we introduce the regularization methods in Sec. 3.4.

3.1 Preliminary: Vanilla Prompt Tuning

Consider a Transformer [40] or its variants used to extract features from an embedded input sequence $\mathbf{x}^0 \in \mathbb{R}_{s \times d_x}$, where s is the sequence length and d_x is the embedding dimension of the Transformer. Prompt-tuning¹ freezes all pre-trained model weights and optimize a small amount of continuous embeddings (*i.e.*, prompts) $\mathbf{P} \in \mathbb{R}_{l \times d}$ inserted into the input, where l is the number of prompts or “prompt length”. The input of the i -th layer L^i could be denoted as:

$$\hat{\mathbf{x}}^i = [x_0^{i-1}, \mathbf{P}, \mathbf{T}^{i-1}] \quad (1)$$

where $x_0^{i-1} \in \mathbb{R}_{d_x}$ denotes the [CLS] token, $\mathbf{T}^{i-1} \in \mathbb{R}_{s \times d_x}$ is the token embedding from the previous layer, and $[\cdot, \cdot]$ denotes the concatenation operation.

¹ In this paper we assume that soft prompts are applied to all layers, which corresponds to “VPT-deep” in CV and “prefix-tuning” in NLP.

Succinctly, prompt tuning works by biasing the pretrained attention pattern in each Transformer layers [32]. As opposed to fine-tuning, this biasing has strictly limited expressiveness [32, 42], meaning that there are tasks that are unlearnable even with $l \rightarrow \infty$. The empirical expressiveness of vanilla prompting is even lower than its theoretical upper bound, due to competing optimization when $l > 1$, as postulated by Petrov *et al.* [32]. In other words, although longer prompts provide the model with more capability, finding such a long prompt becomes challenging, and a suboptimal long prompt can lead to performance degradation. In this paper, we do not aim to increase the theoretical upper bound of prompt-tuning; instead, we approach the problem by narrowing the gap between its empirical and theoretical expressiveness.

3.2 Conditional Prompt Tuning for Multimodal Fusion

Previous prompt-based multimodal fusion methods [21, 22] optimize a global prompt that is shared across all instances. However, this approach neglects the interplay between different modalities. With paired multimodal input as a prior, we aim to condition the prompting of one modality on the other for more adaptive and efficient transfer learning.

Sequential Pipeline. A sequential pipeline for multimodal fusion is adopted to achieve prompt conditioning. Specifically, let (x, y) represent a pair of multimodal inputs, and \mathcal{E}_y be the encoder of modality y . Depending on the intrinsic of the specific task, a fusion direction could be assigned from the complementary modality to the main modality, and the proposed method will be used for tuning the main modality only. Without loss of generality, we consider x to be the main modality in the following discussion.

Prompt Disentanglement. Based on the sequential fusing pipeline, we disentangle the vanilla prompt vector \mathbf{P} used in Eqn. 1 into three types of specialized prompts $[\mathbf{P}_s, \mathbf{P}_d, P_m]$. The static prompt $\mathbf{P}_s \in \mathbb{R}_{l \times d_x}$ is a globally-shared prompt vector that is non-conditional to input. To synthesize the dynamic prompt $\mathbf{P}_d \in \mathbb{R}_{l \times d_x}$, we first extract the global-level feature from the complementary modality $\mathcal{E}_y(y) = \psi_y \in \mathbb{R}_{d_y}$, and utilize a MoPE module $R(\cdot)$ to synthesize the instance-wise dynamic prompt (entailed in Sec 3.3). Additionally, we apply a lightweight mapper $f_m(\cdot)$ to map the complementary feature ψ_y into a single prompt $P_m \in \mathbb{R}_{d_x}$, which injects fine-grained cross-modal information. In summary, the input of layer L^i of \mathcal{E}_x becomes:

$$\hat{\mathbf{x}}^i = [x_0^{i-1}, \underbrace{\mathbf{P}_s, R(\psi_y), f_m(\psi_y)}_{\text{Disentangled prompts}}, \mathbf{T}^{i-1}] \quad (2)$$

It is important to note that our three types of prompting serve as a plug-in module to replace the vanilla prompt vector of the main modality, while treating the encoder of the complementary modality \mathcal{E}_y as a black-box for modularity. The whole process is illustrated in Fig. 2-(a).

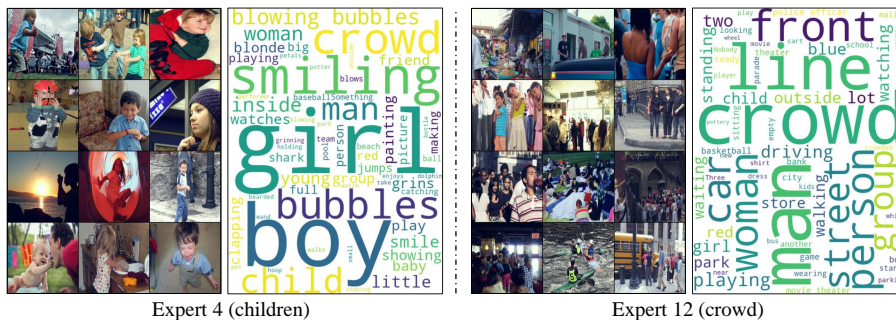


Fig. 3: Interpretable prompting through MoPE routing. Different experts in MoPE learn to specialize in specific types concepts. In this example, expert-4 is specialized for children while expert-12 focuses on crowds.

3.3 Mixture of Prompt Experts

As length-scaling has been proven ineffective due to quick saturation and over-length deterioration, we propose to fix the prompt length used in attention to suppress the negative impact of longer prompts. To inject more learnable parameters into the framework and increase the expressiveness of the prompts, we condition the prompts on multiple prompt experts for end-to-end training.

Prompt as Expert. We randomly initialize k prompt experts and their associated *routing embedding* $\{(\mathbf{E}_j, \mathbf{v}_j)\}_{j=1}^k$ to be optimized end-to-end in each prompt-tuned Transformer layer L^i . For each pair, $\mathbf{E}_i \in \mathbb{R}_l \times d$ is the expert and $\mathbf{v}_i \in \mathbb{R}_{d_r}$ is the routing embedding, where d_r is dimension of routing embedding.

Multimodal Expert Routing. In multimodal tasks, missing information from either modality can lead to ambiguous and incorrect results. Therefore, we route each instance based on representations from both modalities. Specifically, for layer L^i , we apply a layer-wise learned linear transformation $\mathbf{W}_y^i \in \mathbb{R}_{d_y \times d_c}$ to get the cross-modal routing embedding based on cross-modal feature ψ_y , where d_c is the embedding dimension for cross-modal routing. We also utilize the global-level feature from previous layer L^{i-1} to compute a inter-modal routing embedding through $\mathbf{W}_x^i \in \mathbb{R}_{d_x \times d_i}$, where d_i is the inter-modal routing embedding, and $d_i + d_c = d_r$. Finally, we concatenate both embeddings along the embedding dimension to get an adjoint embedding $\mathbf{k} \in \mathbb{R}_{d_r}$, and dot product them with the routing embedding of all available experts. The routing score \mathbf{r} is calculated by:

$$\mathbf{k} = [\psi_y \mathbf{W}_y^i, x_0^i \mathbf{W}_x^i], \quad \mathbf{r}_j = \frac{\exp(\mathbf{k}^\top \mathbf{v}_j / \tau + \epsilon)}{\sum_{n=1}^k \exp(\mathbf{k}^\top \mathbf{v}_n / \tau + \epsilon)} \quad (3)$$

where $\tau = 0.1$ is the temperature hyper-parameter, and ϵ is sampled noise [36]. The dynamic prompt is calculated by a convex combination of all experts at this layer according to the routing score:

$$\mathbf{P}_d = \sum_{j=1}^k \mathbf{r}_j \mathbf{E}_j \quad (4)$$

3.4 Regularizing Expert Routing

The proposed MoPE scales up vanilla prompt tuning by dividing the problem space into subspaces governed by specialized experts. However, we empirically found that a few experts tend to dominate across all instances during training, resulting in non-specialization. This phenomenon is self-reinforcing and is due to degenerated routing, where experts receiving high scores during initialization are exposed to larger gradient scales, causing them to be selected more frequently during optimization [5, 38]. In this section, we introduce methods to circumvent this issue and aid expert specialization.

Orthogonal Routing Embedding. Inspired by the analysis of degenerated routing, we freeze the routing embeddings to avoid self-reinforcement. We find that an orthogonal initialized [37] and non-learnable routing embedding $\{\mathbf{v}\}_{j=1}^k$ performs as well as (and even slightly better than) learned embeddings, while requiring fewer trainable parameters.

Importance Loss. To aid expert specialization, we add an additional importance loss [36, 38] to penalize dominant experts. For a batch of input $\mathbf{B} = \{(x_0, y_0), (x_1, y_1), \dots, (x_b, y_b)\}$, the importance of expert- j is defined as the summed routing score in this batch. The importance loss is calculated as the mean coefficient of variation of all experts’ importance averaged across all layers::

$$\text{Imp}(\mathbf{E}_j) = \sum_{(x,y) \in \mathbf{B}} \mathbf{r}_j, \quad \mathcal{L}_{imp} = \text{stopgrad} \left(\left(\frac{\text{std}(\{\text{Imp}(\mathbf{E}_j)\}_j^k)}{\text{mean}(\{\text{Imp}(\mathbf{E}_j)\}_j^k)} \right)^2 ; \gamma \right) \quad (5)$$

where $\text{stopgrad}(\cdot)$ is the stop-gradient operator to prevent error propagation of this loss term when the coefficient of variation is less than a pre-defined threshold $\gamma = 0.1$. While this loss was initially proposed for balancing computational budgets [36, 38], we adapt its use for promoting expert specialization. We add an additional threshold constraint due to our instance-wise routing, which is more likely to have a larger coefficient of variation than per-token routing.

4 Experiments

4.1 Implementation Details

Architecture Details. For all experiments, unless otherwise specified, we use Swin-B [28] as the vision encoder and Bert-base [3] as the text encoder. Vision is used as main modality. Following the experiment setup in [11, 21], we also finetune a linear head for each dataset. We implement the mapper $f_m(\cdot)$ as a two-layer MLP with GeLU [9] nonlinearity. Regarding prompt tuning, we use

$l = 6$ prompts and $k = 16$ experts by default, and the tunable prompt is applied to all layers of the main modality encoder. Vanilla prompt tuning [20] with $l' = 4$ is used to tune the complementary modality.

Training Details. All images are resized and cropped to the size of 224×224 . All models are trained for 15 epochs, using the AdamW [29] optimizer with a learning rate of 4×10^{-4} for vision and 5×10^{-4} for text. We use a constant step decay scheduler that scales the learning rate at epochs 3 and 6 by a factor of $\gamma = 0.4$. All models are trained on a server with a RTX4090 GPU. The mean and standard deviation of metrics, measured over 4 different experiments are reported when possible.

4.2 Datasets

MM-IMDB [1] is a multimodal movie classification dataset. It consists of 25,956 image-text pairs, where each pair includes a movie poster and a plot summary. The dataset supports multi-label genre classification across a spectrum of 23 genres with a long-tail distribution.

UPMC Food-101 [41] is a comprehensive multimodal dataset designed for fine-grained recipe classification with 90,840 image-text pairs for 101 food classes.

SNLI-VE [43] is a large-scale multimodal dataset with 565,286 image-text pairs. The task for this dataset is visual entailment, which requires the model to infer whether a hypothesis matches the given premise. In our experiments, following [21], we only use the image premise. However, it is worth noting that some other works may also include the text premise.

4.3 Compared Methods

First, we compare our method with several baselines for multimodal fusion.

ImgOnly / TextOnly. Only fine-tune one encoder, and the input of the other modality is discarded.

P-ImgOnly / P-TextOnly. Only prompt-tune one encoder, and the input of the other modality is discarded.

LateConcat. This baseline involves fine-tuning both encoders, concatenating their features, and learn a linear head for classification.

P-LateConcat. Similar as **LateConcat** but prompt-tune each encoder instead of fine-tuning. However, the linear head is still fine-tuned.

SequentialFuse. This method first extracts features from the complementary modality and maps them to the embedding space of the main modality encoder in the same way as our mapped prompt for end-to-end training. Both encoders are fine-tuned. This is a strong baseline that can be considered as our method without MoPE, but with all parameters fine-tuned.

P-SequentialFuse. Prompt-tune each encoders in **SequentialFuse**.

For a fair comparison, all the prompt-tuning methods listed above use the same prompt length ($l = 6$) as our method. In addition to these baselines, we also compare our methods with existing prompt-based fusion methods, including

Table 1: Quantitative results on three multimodal dataset. We compare all baseline methods, existing prompt-based fusion methods, and our method with different expert numbers. Our method achieve state-of-the-art performance and parameter-efficiency. (†): Our implementation with prefix-tuning.

	Method	Param	SNLI-VE(†)	Food-101(†)	MM-IMDB(†)
<i>finetuning</i>	ImgOnly	86.9M	33.34±.03	75.64±.21	39.21±.32/53.85±.21
	TextOnly	109.0M	69.58±.24	86.92±.21	58.80±.31/65.37±.13
	LateConcat	196.0M	72.01±.23	93.19±.21	60.43±.68/67.77±.36
	SequentialFuse	197.0M	74.28±.46	93.73±.16	59.22±.38/66.34±.19
	MMBT [15]	196.5M	67.58	94.10	60.80/66.10
<i>prompt-tuning</i>	P-ImgOnly	0.1M	33.34±.01	76.65±.07	33.70±.55/50.04±.27
	P-TextOnly	0.1M	64.86±.32	81.01±.50	52.19±.32/61.16±.43
	P-LateConcat	1.3M	64.29±.28	90.27±.40	56.95±.37/64.23±.26
	P-SequentialFuse	1.1M	65.01±.18	81.27±.22	55.57±.63/63.98±.35
	P-MMBT [21]	0.9M	67.58	81.07	52.95/59.30
	PromptFuse [22]	<0.1M	64.53	82.21	48.59/54.49
	BlindPrompt [22]	<0.1M	65.54	84.56	50.18/56.46
	PromptFuse(†) [22]	0.1M	64.94	82.14	50.78/60.96
	PMF [21]	2.5M	71.92	91.51	58.77/64.51
	Ours (ViT-b, $k = 4$)	1.6M	73.47±.11	91.55±.12	62.37±.35/68.73±.24
Ours (Swin-b, $k = 4$)	1.6M	73.14±.21	91.54±.21	61.93±.37/68.19±.14	
Ours (Swin-b, $k = 16$)	2.6M	73.59±.15	92.05±.11	62.01±.21/68.24±.12	

MMBT [15], Frozen [39], PromptFuse and BlindPrompt [22], and PMF [21]. Among these methods, the setting in PromptFuse [22] is the most similar to ours, as it also assumes one modality to be a black-box.

4.4 Main Results

The quantitative results of all baselines, compared methods, and our method with different expert numbers k are summarized in Tab 1. The metric on SNLI-VE and Food-101 is accuracy (%), and MM-IMDB is F1-Macro and F1-Micro (%). We also list the number of trainable parameters (million) for each method.

Our method outperforms all prompt-based methods, and is competitive with fine-tuning. Specifically, when compared with the fine-tuning baselines, SequentialFuse and LateConcat, our method delivers competitive accuracy on the Food-101 dataset and superior results on the SNLI-VE and MM-IMDB datasets, while requiring as few as 0.8% of the trainable parameters.

Apart from surpassing baselines, the proposed method also outperforms existing prompt-based fusion methods, including PromptFuse [22], BlindPrompt [22], and PMF [21]. Notably, our method outperforms the current SOTA, PMF [21], by a significant margin on all datasets, while requiring 37% fewer parameters. Moreover, PMF assumes both encoders share the same Transformer architecture. By contrast, our method has weaker assumptions, which could be easily extended to any Transformer-based architecture, such as ViT [4] and Swin [28].

Table 2: Ablation on three types of prompt disentanglement. The results from all combinations of mapped prompt, dynamic prompt, and static prompt are presented. Our full method with all prompts achieves the best result.

Prompt	SNLI-VE(\uparrow)	Food-101(\uparrow)	MM-IMDB(\uparrow)
$[\mathbf{P}_s]$	33.34 \pm .01	76.65 \pm .07	33.70 \pm .55/50.04 \pm .27
$[\mathbf{P}_d]$	64.26 \pm .41	74.79 \pm .38	46.54 \pm .77/59.71 \pm .35
$[P_m]$	33.47 \pm .32	73.06 \pm .12	24.84 \pm .14/45.10 \pm .32
$[\mathbf{P}_s, \mathbf{P}_d]$	66.76 \pm .26	75.13 \pm .14	49.09 \pm .43/60.89 \pm .37
$[\mathbf{P}_s, P_m]$	65.01 \pm .18	81.27 \pm .22	55.57 \pm .63/63.98 \pm .35
$[\mathbf{P}_d, P_m]$	71.39 \pm .59	91.21 \pm .16	60.15 \pm .37/67.14 \pm .17
$[\mathbf{P}_s, \mathbf{P}_d, P_m]$	73.59\pm.15	92.05\pm.11	62.01\pm.21/68.24\pm.12

4.5 Qualitative Result of MoPE Routing

During end-to-end tuning, prompt experts in MoPE spontaneously specialize in different concepts. Fig. 3 presents two examples of this specialization. Specifically, we visualize the expert with the highest score as the routed expert for each instance pair. In the provided examples, we observe that expert-4 specialize in children-related concepts, while expert-12 focuses on crowds. These examples also demonstrate the interpretability of our MoPE-based prompting, as opposed to black-box conditional prompt such as CoOp [50] and CoCoOp [49]. We encourage readers for a more comprehensive visualizations in Appendix C.2.

5 Analysis and Discussion

In this section, we systematically analyze the effects of our proposed design through ablation studies. We show that our MoPE-based fusion method is more adaptive and scalable for multimodal fusion compared to existing approaches.

Our three-types of disentangled prompts are collaborative. We first ablate each type of prompt in our prompt disentanglement, and the results are summarized in Tab. 2. Our full method achieves the best performance, indicating that the prompts collaborate effectively with each other. Specifically, the dynamic prompt is essential for multimodal fusion as it learns the interplay between different modalities. This is in contrast with previous methods [22, 39, 45], where each modality do not explicitly interact. Adding the dynamic prompt induces a significant gain of 13.5%, 13.26, 8.4%/6.5% on all datasets. Without the mapped prompt, the fine-grained information from complimentary modality is lost, leading to a significant drop in all datasets. The static prompt is also necessary, serving as a special expert that is always routed. Adding this special expert allows the other experts to focus more on capturing instance-level features, resulting in a slight performance gain.

Expert-scaling is more expressive than length-scaling. To study the expressiveness of MoPE, we compare expert-scaling with length-scaling. Our starting point for MoPE is $l = 6$ prompts and $k = 2$ experts (when $k \leq 1$, MoPE

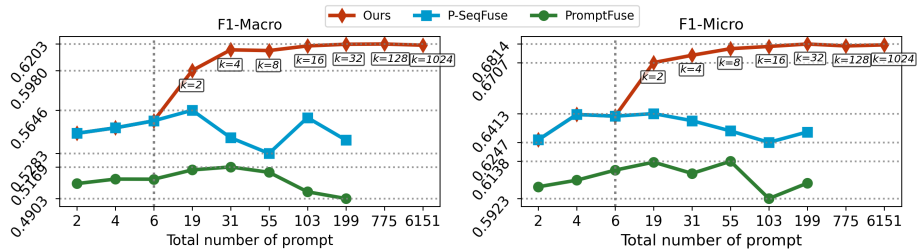


Fig. 4: More experts v.s. longer prompts. We compare increasing the number of experts, k , versus lengthen prompt, l . Expert-scaling consistently outperforms length-scaling, exhibiting a linear growth trend and do not deteriorate even when $k \rightarrow \infty$. Conversely, excessive prompt length has a negative impact on accuracy and speed.

degenerate into vanilla prompt), which account for $(2 + 1) \times 6 + 1 = 19$ tunable prompts in total per-layer. We increase the number of k , and at each step we also report the result of simply increasing l in vanilla prompt, up to the same total number of prompts. The results are summarised in Fig. 4.

As illustrated in the figure, adding the MoPE design with as few as $k = 2$ experts boosts performance, and increasing the number of experts leads to a monotonic performance improvement. Although our method may also saturate when the number of experts becomes excessive, it does not face the over-length deterioration issue observed in vanilla prompt tuning. In contrast, merely augmenting the number of prompts l in vanilla prompt tuning does not lead to a linear performance improvement and is prone to performance deterioration. This observation is consistent with previous findings [11, 14, 20, 44]. This makes the prompt length l a hyperparameter that is difficult to tune manually. In addition to accuracy considerations, longer prompts in vanilla prompt tuning can exacerbate computational overhead due to the quadratic time complexity of self-attention. This is why we cannot experiment with $l > 199$ for the other two methods. On the other hand, MoPE scales by conditioning the dynamic prompt on more experts while maintaining a fixed length of learnable prompts during self-attention. As a result, our method maintains a nearly constant time complexity.

MoPE scales better when more training data is available. Previous prompting methods have been shown to not scale well with respect to increased training data [7, 22, 39, 44]. We study how the proposed MoPE method performs on different data scales to assess its scalability. Specifically, we sub-sample the training-set with different shots to represent a range of low-shot to high-shot learning scenarios. We then train our method and other prompt-tuning and fine-tuning methods with the same subsampled data. The mean accuracy and F1-Micro score on SNLI-VE and MM-IMDB, respectively, are reported in Fig. 5.

As the figure shows, our MoPE-based method is the most scalable, achieving superior results across all data scales. Specifically, we consistently match the results of the fine-tuning method, SequentialFuse, on the SNLI-VE dataset, and

Table 3: Result of dense routing v.s. sparse routing. Dense routing achieves slightly better results on all three datasets.

Routing	SNLI-VE ↑	Food-101 ↑	MM-IMDB ↑
Dense	73.55	91.74	62.01/68.25
Sparse	71.15	90.89	60.28/66.01

Table 4: Different way of generating routing embedding. Frozen routing embedding with orthogonal initialization is as good as learned one.

Routing Embed	SNLI-VE ↑	Food-101 ↑	MM-IMDB ↑
Frozen	73.55	91.74	62.01/68.25
Learned	73.13	91.20	61.64/67.97

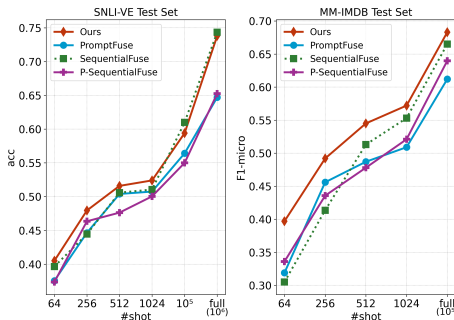


Fig. 5: Scaling performance with increased training data. We show the performance of our method and representative methods as we progressively increase the amount of training data, or “#shots”. Our method outperform other prompt-tuning methods at all data scales.

we achieve superior results on the MM-IMDB dataset. By contrast, the method based on vanilla-prompt does not scale well with respect to increased training data, and there is a consistent performance gap between ours and the compared method. This performance gap becomes more significant on larger datasets, such as when training with 10^5 shots or using the full training set.

Dense routing with frozen routing embedding achieves the best result. Previous MoE with FFN acting as experts usually employ a sparse gating function that only select one or a few experts per token, while we use a dense router (Eqn. 4) that weigh all experts. To compare the effect, we follow [36] to implement a sparse router by adding a Top-1 gate: $\mathbf{r}' = \text{TOP}_1(\mathbf{r})$.

The results of using sparse routing versus dense routing are reported in Tab. 3. Our experiments indicate that using the dense router yields marginally better results.

To further understand how dense routing benefits the model, we evaluated the degree of uncertainty in routing by calculating the empirical entropy of the routing score $\mathcal{H}(\mathbf{r}) = -\sum_{i=1}^n r_i \log_2(r_i)$, averaged across training batches and all layers. In essence, high entropy indicates that routing behaves more randomly. The relationship between entropy and optimization steps is illustrated in Fig. 6. As demonstrated in the figure, dense routing is more deterministic.

In addition to routing sparsity, we also investigate the effect of using frozen routing embeddings. As Tab. 4 shows, fixed routing embedding could achieve the same result as the trained one.

Importance loss aids expert specialization. The importance loss is crucial for avoiding degenerate routing solutions and, consequently, aids expert specialization. In Fig. 7, we visualize how the importance of each expert (*i.e.*, average routing score) changes when training on the SNLI-VE dataset. Without

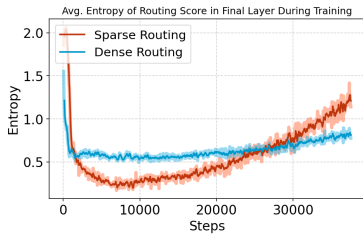


Fig. 6: Routing determinism. We show the entropy of routing score during training. Dense routing are more deterministic as optimization progress. Better viewed with color.

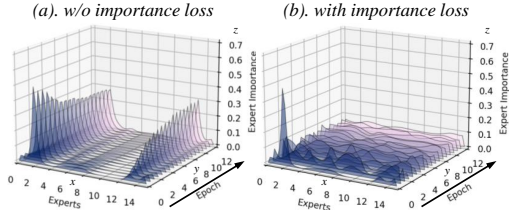


Fig. 7: Effect of the importance loss. We visualize how the importance (z-axis) of all experts (x-axis) in the last Transformer layer changes during training (y-axis). (a) Without importance loss, only a few experts are used throughout training (b) The importance loss ensures balanced utilization of all experts.

the importance loss, routing adheres to its initial state, resulting in a skewed distribution where a few experts dominate. The importance loss allows other experts to be used by penalizing highly unbalanced expert importance.

Our fusion method are highly modular. Our method abstracts the complementary modality as a black-box, allowing high modality of both modalities. In particular, our method allow arbitrary models to be seamless plug-in for multimodal fusion. We give some results in Tab. 5.

How could MoPE be more expressive & Limitations. We have demonstrated that the MoPE-based method is more expressive for multimodal fusion. Compared with existing prompt-based methods, our approach scales better with data and trainable parameters. This increased expressiveness comes from two factors. First, the prompts used in previous methods are not adaptive, meaning that a single prompt is used for all instances. Finding a instance-wise optimal prompt could lead to better results. Secondly, we scale the prompt by using more experts, since a long prompt can be difficult to optimize [32] for optimal performance. By doing so, we shift the difficulty from learning a universal long prompt to learning a parameterized router with multiple short prompts. As a result, our empirical expressiveness is closer to the theoretical upper bound of prompt-tuning.

Despite improving empirical expressiveness, our prompt still functions in the same way as vanilla prompts during attention, resulting in same theoretical upper-bound of expressiveness. This is also reflected by the small gap between ours and fine-tuning in large datasets such as SNLI-VE and UPMC Food-101. Future studies could focus on designing a more expressive prompting technique.

Architecture	Tuning	MM-IMDB (\uparrow)
BoW*	Fine-tune	48.20/57.50
Bert [3]	Frozen	58.86/66.13
GPT-2 [35]	Frozen	34.03/50.84
Longformer [3]	Bitfit [46]	60.34/67.27

Table 5: Our fusing method is highly modular. We treat complementary modality as black-box, allowing different models to be plug-in for fusion. (*): Bag-of-word initialized with Bert word embeddings.

6 Conclusion

In this paper, we enhance the scalability and adaptivity of prompts used in multimodal fusion. Our method involves disentangling the prompt into static and dynamic components to enable instance-adaptive prompt learning. To circumvent performance deterioration due to overly long prompts, we introduce the mixture-of-prompt-expert technique, which improves the expressiveness of prompt-tuning. Extensive experiments demonstrate that our method is highly parameter-efficient and scales better with dataset size and prompt length. We have also shown that our method is interpretable and highly modular.

References

1. Arevalo, J., Solorio, T., Montes-y Gómez, M., González, F.A.: Gated multimodal units for information fusion. arXiv preprint arXiv:1702.01992 (2017) [3](#), [9](#)
2. Bahng, H., Jahanian, A., Sankaranarayanan, S., Isola, P.: Exploring visual prompts for adapting large-scale models. arXiv preprint arXiv:2203.17274 (2022) [4](#)
3. Devlin, J., Chang, M.W., Lee, K., Toutanova, K.: Bert: Pre-training of deep bidirectional transformers for language understanding. arXiv preprint arXiv:1810.04805 (2018) [1](#), [8](#), [14](#), [19](#)
4. Dosovitskiy, A., Beyer, L., Kolesnikov, A., Weissenborn, D., Zhai, X., Unterthiner, T., Dehghani, M., Minderer, M., Heigold, G., Gelly, S., et al.: An image is worth 16x16 words: Transformers for image recognition at scale. arXiv preprint arXiv:2010.11929 (2020) [1](#), [10](#), [19](#)
5. Eigen, D., Ranzato, M., Sutskever, I.: Learning factored representations in a deep mixture of experts. arXiv preprint arXiv:1312.4314 (2013) [8](#)
6. Fedus, W., Zoph, B., Shazeer, N.: Switch transformers: Scaling to trillion parameter models with simple and efficient sparsity. *The Journal of Machine Learning Research* **23**(1), 5232–5270 (2022) [4](#)
7. Gao, Y., Shi, X., Zhu, Y., Wang, H., Tang, Z., Zhou, X., Li, M., Metaxas, D.N.: Visual prompt tuning for test-time domain adaptation. arXiv preprint arXiv:2210.04831 (2022) [2](#), [4](#), [12](#)
8. Goyal, Y., Khot, T., Summers-Stay, D., Batra, D., Parikh, D.: Making the v in vqa matter: Elevating the role of image understanding in visual question answering. In: *Proceedings of the IEEE conference on computer vision and pattern recognition*. pp. 6904–6913 (2017) [25](#)
9. Hendrycks, D., Gimpel, K.: Gaussian error linear units (gelus). arXiv preprint arXiv:1606.08415 (2016) [8](#)
10. Hu, E.J., Shen, Y., Wallis, P., Allen-Zhu, Z., Li, Y., Wang, S., Wang, L., Chen, W.: Lora: Low-rank adaptation of large language models. arXiv preprint arXiv:2106.09685 (2021) [4](#)
11. Jia, M., Tang, L., Chen, B.C., Cardie, C., Belongie, S., Hariharan, B., Lim, S.N.: Visual prompt tuning. In: *European Conference on Computer Vision*. pp. 709–727. Springer (2022) [2](#), [4](#), [8](#), [12](#), [19](#), [24](#)
12. Jiang, R., Liu, L., Chen, C.: Clip-count: Towards text-guided zero-shot object counting. In: *Proceedings of the 31st ACM International Conference on Multimedia*. pp. 4535–4545 (2023) [4](#)

13. Kazemzadeh, S., Ordonez, V., Matten, M., Berg, T.: Referitgame: Referring to objects in photographs of natural scenes. In: Proceedings of the 2014 conference on empirical methods in natural language processing (EMNLP). pp. 787–798 (2014) [23](#)
14. Khattak, M.U., Rasheed, H., Maaz, M., Khan, S., Khan, F.S.: Maple: Multi-modal prompt learning. In: Proceedings of the IEEE/CVF Conference on Computer Vision and Pattern Recognition. pp. 19113–19122 (2023) [2](#), [4](#), [12](#)
15. Kiela, D., Bhooshan, S., Firooz, H., Perez, E., Testuggine, D.: Supervised multimodal bitransformers for classifying images and text. arXiv preprint arXiv:1909.02950 (2019) [10](#)
16. Kim, Y., Li, Y., Moitra, A., Panda, P.: Do we really need a large number of visual prompts? arXiv preprint arXiv:2305.17223 (2023) [2](#), [4](#)
17. Kirillov, A., Mintun, E., Ravi, N., Mao, H., Rolland, C., Gustafson, L., Xiao, T., Whitehead, S., Berg, A.C., Lo, W.Y., et al.: Segment anything. arXiv preprint arXiv:2304.02643 (2023) [1](#)
18. Lepikhin, D., Lee, H., Xu, Y., Chen, D., Firat, O., Huang, Y., Krikun, M., Shazeer, N., Chen, Z.: Gshard: Scaling giant models with conditional computation and automatic sharding. arXiv preprint arXiv:2006.16668 (2020) [4](#)
19. Lester, B., Al-Rfou, R., Constant, N.: The power of scale for parameter-efficient prompt tuning. arXiv preprint arXiv:2104.08691 (2021) [2](#), [4](#)
20. Li, X.L., Liang, P.: Prefix-tuning: Optimizing continuous prompts for generation. arXiv preprint arXiv:2101.00190 (2021) [2](#), [4](#), [9](#), [12](#), [19](#)
21. Li, Y., Quan, R., Zhu, L., Yang, Y.: Efficient multimodal fusion via interactive prompting. In: Proceedings of the IEEE/CVF Conference on Computer Vision and Pattern Recognition. pp. 2604–2613 (2023) [2](#), [4](#), [6](#), [8](#), [9](#), [10](#), [19](#), [24](#)
22. Liang, S., Zhao, M., Schütze, H.: Modular and parameter-efficient multimodal fusion with prompting. arXiv preprint arXiv:2203.08055 (2022) [2](#), [4](#), [6](#), [10](#), [11](#), [12](#)
23. Lin, J., Chang, J., Liu, L., Li, G., Lin, L., Tian, Q., Chen, C.w.: Being comes from not-being: Open-vocabulary text-to-motion generation with wordless training. In: Proceedings of the IEEE/CVF conference on computer vision and pattern recognition. pp. 23222–23231 (2023) [4](#)
24. Lin, T.Y., Maire, M., Belongie, S., Hays, J., Perona, P., Ramanan, D., Dollár, P., Zitnick, C.L.: Microsoft coco: Common objects in context. In: Computer Vision–ECCV 2014: 13th European Conference, Zurich, Switzerland, September 6–12, 2014, Proceedings, Part V 13. pp. 740–755. Springer (2014) [23](#)
25. Liu, L., Chang, J., Yu, B.X., Lin, L., Tian, Q., Chen, C.W.: Prompt-matched semantic segmentation. arXiv preprint arXiv:2208.10159 (2022) [4](#)
26. Liu, L., Chen, J., Wu, H., Li, G., Li, C., Lin, L.: Cross-modal collaborative representation learning and a large-scale rgbt benchmark for crowd counting. In: Proceedings of the IEEE/CVF conference on computer vision and pattern recognition. pp. 4823–4833 (2021) [1](#)
27. Liu, X., Ji, K., Fu, Y., Tam, W.L., Du, Z., Yang, Z., Tang, J.: P-tuning v2: Prompt tuning can be comparable to fine-tuning universally across scales and tasks. arXiv preprint arXiv:2110.07602 (2021) [2](#)
28. Liu, Z., Lin, Y., Cao, Y., Hu, H., Wei, Y., Zhang, Z., Lin, S., Guo, B.: Swin transformer: Hierarchical vision transformer using shifted windows. In: Proceedings of the IEEE/CVF international conference on computer vision. pp. 10012–10022 (2021) [1](#), [8](#), [10](#), [19](#)
29. Loshchilov, I., Hutter, F.: Decoupled weight decay regularization. arXiv preprint arXiv:1711.05101 (2017) [9](#)

30. Ma, J., Wang, B.: Segment anything in medical images. arXiv preprint arXiv:2304.12306 (2023) [1](#)
31. Mustafa, B., Riquelme, C., Puigcerver, J., Jenatton, R., Houlsby, N.: Multimodal contrastive learning with limoe: the language-image mixture of experts. *Advances in Neural Information Processing Systems* **35**, 9564–9576 (2022) [4](#)
32. Petrov, A., Torr, P.H., Bibi, A.: When do prompting and prefix-tuning work? a theory of capabilities and limitations. arXiv preprint arXiv:2310.19698 (2023) [2](#), [4](#), [6](#), [14](#), [20](#)
33. Qin, G., Eisner, J.: Learning how to ask: Querying lms with mixtures of soft prompts. arXiv preprint arXiv:2104.06599 (2021) [4](#)
34. Radford, A., Kim, J.W., Hallacy, C., Ramesh, A., Goh, G., Agarwal, S., Sastry, G., Askell, A., Mishkin, P., Clark, J., et al.: Learning transferable visual models from natural language supervision. In: *International conference on machine learning*. pp. 8748–8763. PMLR (2021) [1](#)
35. Radford, A., Wu, J., Child, R., Luan, D., Amodei, D., Sutskever, I., et al.: Language models are unsupervised multitask learners. *OpenAI blog* **1**(8), 9 (2019) [1](#), [14](#)
36. Riquelme, C., Puigcerver, J., Mustafa, B., Neumann, M., Jenatton, R., Susano Pinto, A., Keyzers, D., Houlsby, N.: Scaling vision with sparse mixture of experts. *Advances in Neural Information Processing Systems* **34**, 8583–8595 (2021) [4](#), [7](#), [8](#), [13](#)
37. Saxe, A.M., McClelland, J.L., Ganguli, S.: Exact solutions to the nonlinear dynamics of learning in deep linear neural networks. arXiv preprint arXiv:1312.6120 (2013) [8](#)
38. Shazeer, N., Mirhoseini, A., Maziarz, K., Davis, A., Le, Q., Hinton, G., Dean, J.: Outrageously large neural networks: The sparsely-gated mixture-of-experts layer. arXiv preprint arXiv:1701.06538 (2017) [4](#), [8](#)
39. Tsimpoukelli, M., Menick, J.L., Cabi, S., Eslami, S., Vinyals, O., Hill, F.: Multimodal few-shot learning with frozen language models. *Advances in Neural Information Processing Systems* **34**, 200–212 (2021) [2](#), [4](#), [10](#), [11](#), [12](#)
40. Vaswani, A., Shazeer, N., Parmar, N., Uszkoreit, J., Jones, L., Gomez, A.N., Kaiser, Ł., Polosukhin, I.: Attention is all you need. *Advances in neural information processing systems* **30** (2017) [5](#)
41. Wang, X., Kumar, D., Thome, N., Cord, M., Precioso, F.: Recipe recognition with large multimodal food dataset. In: *2015 IEEE International Conference on Multimedia & Expo Workshops (ICMEW)*. pp. 1–6. IEEE (2015) [3](#), [9](#), [23](#)
42. Wang, Y., Chauhan, J., Wang, W., Hsieh, C.J.: Universality and limitations of prompt tuning. arXiv preprint arXiv:2305.18787 (2023) [2](#), [4](#), [6](#), [20](#)
43. Xie, N., Lai, F., Doran, D., Kadav, A.: Visual entailment: A novel task for fine-grained image understanding. arXiv preprint arXiv:1901.06706 (2019) [3](#), [9](#)
44. Yang, H., Lin, J., Yang, A., Wang, P., Zhou, C., Yang, H.: Prompt tuning for generative multimodal pretrained models. arXiv preprint arXiv:2208.02532 (2022) [2](#), [4](#), [12](#)
45. Yang, Z., Gan, Z., Wang, J., Hu, X., Lu, Y., Liu, Z., Wang, L.: An empirical study of gpt-3 for few-shot knowledge-based vqa. In: *Proceedings of the AAAI Conference on Artificial Intelligence*. vol. 36, pp. 3081–3089 (2022) [2](#), [4](#), [11](#)
46. Zaken, E.B., Ravfogel, S., Goldberg, Y.: Bitfit: Simple parameter-efficient fine-tuning for transformer-based masked language-models. arXiv preprint arXiv:2106.10199 (2021) [14](#)
47. Zang, Y., Li, W., Zhou, K., Huang, C., Loy, C.C.: Unified vision and language prompt learning. arXiv preprint arXiv:2210.07225 (2022) [4](#)

48. Zheng, S., Lu, J., Zhao, H., Zhu, X., Luo, Z., Wang, Y., Fu, Y., Feng, J., Xiang, T., Torr, P.H., et al.: Rethinking semantic segmentation from a sequence-to-sequence perspective with transformers. In: Proceedings of the IEEE/CVF conference on computer vision and pattern recognition. pp. 6881–6890 (2021) [24](#)
49. Zhou, K., Yang, J., Loy, C.C., Liu, Z.: Conditional prompt learning for vision-language models. In: Proceedings of the IEEE/CVF Conference on Computer Vision and Pattern Recognition. pp. 16816–16825 (2022) [4](#), [11](#)
50. Zhou, K., Yang, J., Loy, C.C., Liu, Z.: Learning to prompt for vision-language models. *International Journal of Computer Vision* **130**(9), 2337–2348 (2022) [2](#), [11](#)
51. Zhu, J., Xia, Y., Wu, L., He, D., Qin, T., Zhou, W., Li, H., Liu, T.Y.: Incorporating bert into neural machine translation. arXiv preprint arXiv:2002.06823 (2020) [1](#)

A Additional Experiment Details

In this section, we provide additional details of our implementation and training.

Prompt Vector. Our prompt implementation closely follows [11]. Specifically, for static prompts and prompt experts, we use uniform initialization $\mathcal{U} \sim (-\eta, \eta)$, where η is calculated according to the embedding dimension and patch size of the Transformer [11]. Dropout with $p = 0.1$ is applied to all prompts. However, we do not use the reparameterization trick for prompts [20], as the gradients of our dynamic prompt and mapped prompt are already rectified by MLPs. For Transformer architectures that employ a window attention mechanism, we duplicate the same prompt and prepend it to all windows for attention calculation, following the approach in [11].

Mapper. The main objective of the mapper is to map representations from dimension y to the embedding dimension of modality x . Generally speaking, the mapper is implemented as a two-block MLP, which shares similarities with previous work [21]. In our experiments, we set the bottleneck dimension as half of the dimension of the complementary representation, i.e., $d_{bot} = \lceil d_y/2 \rceil$. Then, we apply a batch normalization layer and a GeLU activation to obtain a bottleneck feature $\psi_{bot} \in \mathbb{R}^{d_{bot}}$.

After obtaining this bottleneck feature, we apply another MLP to project it to the embedding dimension of d_x . However, some Transformer architectures use inconsistent d_x in their internal layers. For example, in Swin-b [28], the embedding dimension changes from [128, 256, 512, 1024], making it challenging to fit a single MLP. To circumvent this, we instead learn four separate linear projections, each used to project the shared bottleneck feature to different embedding dimensions. As a result, there is one single down-sampling MLP and multiple up-sampling MLPs. To ensure fairness, we also use a similar design in plain Transformers such as ViT [4] and BERT [3].

MoPE. As discussed in the main body of this paper, we learn a per-layer linear projection to obtain the cross-model embedding. Here, we would like to further clarify that this projection weight is not shared with the one used in the mapper. In our experiments, we use $d_c = 8$ and $d_i = 2$, resulting in $d_r = 10$. For the importance loss, we scale it by a factor of 0.01 and apply it together with the task-specific losses.

B Extended Analysis and Discussion

B.1 Analysis on Adaptivity of vanilla prompt and MoPE

In the main body of the paper, we have empirically demonstrated that the dynamic prompt generated by MoPE exhibits greater adaptivity compared to global-shared prompt tuning. In this section, we aim to further characterize and quantify the adaptiveness of different prompt techniques. Through this analysis, we will also provide intuitive insights into the significance of expert specialization in MoPE-based fusion.

Following the approach adopted in previous papers [32, 42], we will focus our analysis on the case of a single prompt within a single Transformer layer. Since our method is designed to generate an effective prompt while leaving the attention calculation the same as previous prompt tuning, our MoPE will only affect the forward behavior up to the calculation of attention map. Therefore, we will concentrate on analyzing how different prompts influence the attention pattern of a pretrained Transformer layer.

Let us define the attention map produced by the self-attention operation as $\mathbf{A}(\mathbf{X}, \mathbf{P})$, which is a function of the input \mathbf{X} and the prompt \mathbf{P} . The objective is to find a prompt \mathbf{P} that enables the attention map $\mathbf{A}(\mathbf{X}, \mathbf{P})$ to closely match the desired target attention pattern for each input instance.

Theorem 1 (Limited Adaptivity of Global-shared Prompt). *Let \mathcal{X} be the input space, and \mathcal{A} be the space of attention matrices. For any input $\mathbf{x} \in \mathcal{X}$, let $\mathcal{A}^*(\mathbf{x}) \subseteq \mathcal{A}$ denote the set of optimal attention patterns that minimize the downstream task loss. Define the attention mapping induced by a prompt \mathbf{P} as $\mathcal{A}(\mathbf{x}, \mathbf{P}) \subseteq \mathcal{A}$. Then, for vanilla prompting with a single shared prompt \mathbf{P} , there exists no $\mathbf{P} \in \mathcal{P}$ such that $\mathcal{A}^*(\mathbf{x}) \subseteq \mathcal{A}(\mathbf{x}, \mathbf{P})$ for all $\mathbf{x} \in \mathcal{X}$, where \mathcal{P} is the prompt space.*

Proof. Let $\mathbf{x}_1, \mathbf{x}_2 \in \mathcal{X}$ be two distinct input instances with disjoint optimal attention sets, i.e., $\mathcal{A}^*(\mathbf{x}_1) \cap \mathcal{A}^*(\mathbf{x}_2) = \emptyset$. Define the attention discrepancy for an instance \mathbf{x} and prompt \mathbf{P} as:

$$\Delta(\mathbf{x}, \mathbf{P}) = \inf_{\mathbf{A} \in \mathcal{A}(\mathbf{x}, \mathbf{P})} \|\mathbf{A} - \mathcal{A}^*(\mathbf{x})\|_{\mathcal{A}} \quad (6)$$

where $\|\cdot\|_{\mathcal{A}}$ is a suitable distance metric on \mathcal{A} .

Let \mathbf{P}_1^* and \mathbf{P}_2^* be the locally optimal prompts for instances \mathbf{x}_1 and \mathbf{x}_2 , respectively, i.e.,

$$\mathbf{P}_1^* = \arg \min_{\mathbf{P} \in \mathcal{P}} \Delta(\mathbf{x}_1, \mathbf{P}) \quad (7)$$

$$\mathbf{P}_2^* = \arg \min_{\mathbf{P} \in \mathcal{P}} \Delta(\mathbf{x}_2, \mathbf{P}) \quad (8)$$

For vanilla prompting with a shared prompt \mathbf{P} , the globally optimal shared prompt $\mathbf{P}_{\text{shared}}^*$ minimizes the accumulated attention discrepancy:

$$\mathbf{P}_{\text{shared}}^* = \arg \min_{\mathbf{P} \in \mathcal{P}} \Delta(\mathbf{x}_1, \mathbf{P}) + \Delta(\mathbf{x}_2, \mathbf{P}) \quad (9)$$

Due to the disjointness of optimal attention sets for each instance, the accumulated attention discrepancy for the globally optimal shared prompt $\mathbf{P}_{\text{shared}}^*$ is lower-bounded by the sum of the locally optimal attention discrepancies for \mathbf{x}_1 and \mathbf{x}_2 :

$$\Delta(\mathbf{x}_1, \mathbf{P}_{\text{shared}}^*) + \Delta(\mathbf{x}_2, \mathbf{P}_{\text{shared}}^*) \geq \Delta(\mathbf{x}_1, \mathbf{P}_1^*) + \Delta(\mathbf{x}_2, \mathbf{P}_2^*) \quad (10)$$

Furthermore, by the limited expressiveness of prompt-tuning [32], we have:

$$\Delta(\mathbf{x}_2, \mathbf{P}_2^*) \geq 0; \Delta(\mathbf{x}_1, \mathbf{P}_1^*) \geq 0 \quad (11)$$

Hence, the following relationship holds:

$$\Delta(\mathbf{x}_1, \mathbf{P}_{\text{shared}}^*) + \Delta(\mathbf{x}_2, \mathbf{P}_{\text{shared}}^*) \geq \Delta(\mathbf{x}_1, \mathbf{P}_1^*) + \Delta(\mathbf{x}_2, \mathbf{P}_2^*) \geq 0 \quad (12)$$

Theorem 2 (Improved Adaptivity of MoPE). *Let $\mathcal{E} = \{\mathcal{E}_1, \mathcal{E}_2, \dots, \mathcal{E}_k\}$ be a set of k expert attention mappings, where each $\mathcal{E}_i : \mathcal{X} \rightarrow \mathcal{A}$ maps an input $\mathbf{x} \in \mathcal{X}$ to a set of attention patterns $\mathcal{E}_i(\mathbf{x}) \subseteq \mathcal{A}$. Define the induced attention mapping of MoPE as:*

$$\mathcal{A}_{\text{MoPE}}(\mathbf{x}, \mathcal{E}, \mathbf{r}) = \left\{ \sum_{i=1}^k r_i(\mathbf{x}) \mathbf{A}_i \mid \mathbf{A}_i \in \mathcal{E}_i(\mathbf{x}), \forall i \right\} \quad (13)$$

where $\mathbf{r}(\mathbf{x}) = [r_1(\mathbf{x}), \dots, r_k(\mathbf{x})]$ are the routing weights for input \mathbf{x} .

Let $\mathcal{X}' \subseteq \mathcal{X}$ be a set of instances. If the convex hull of the expert attention mappings, denoted as:

$$\text{conv}(\mathcal{E}) = \left\{ \sum_{i=1}^k \alpha_i \mathbf{A}_i \mid \mathbf{A}_i \in \mathcal{E}_i(\mathbf{x}), \forall i, \forall \mathbf{x} \in \mathcal{X}', \sum_{i=1}^k \alpha_i = 1, \alpha_i \geq 0 \right\} \quad (14)$$

contains an optimal attention pattern for each instance in \mathcal{X}' , i.e., $\mathcal{A}^*(\mathbf{x}) \subseteq \text{conv}(\mathcal{E}), \forall \mathbf{x} \in \mathcal{X}'$, then there exists a routing score \mathbf{r}^* such that the accumulated attention discrepancy for MoPE under \mathbf{r}^* across instances in \mathcal{X}' is equal to the sum of the optimal instance-wise attention discrepancies, i.e.,

$$\sum_{\mathbf{x} \in \mathcal{X}'} \Delta(\mathbf{x}, \mathcal{E}, \mathbf{r}^*) = \sum_{\mathbf{x} \in \mathcal{X}'} \inf_{\mathbf{A} \in \mathcal{A}^*(\mathbf{x})} \|\mathbf{A} - \mathbf{A}^*\|_{\mathcal{A}} \quad (15)$$

Proof. When there are more experts than instances, i.e. $|\mathcal{X}'| \leq k$, the proof is trivial. This is because the optimal prompt for each instance could simply be “stored” in one or a few experts.

When cardinality of the instances is greater than the number of experts, i.e., $|\mathcal{X}'| > k$. Let $\mathcal{X}' \subseteq \mathcal{X}$ be a set of instances with $|\mathcal{X}'| > k$, and assume that the convex hull of the expert attention mappings, $\text{conv}(\mathcal{E})$, contains an optimal attention pattern for each instance in \mathcal{X}' , i.e., $\mathcal{A}^*(\mathbf{x}) \subseteq \text{conv}(\mathcal{E}), \forall \mathbf{x} \in \mathcal{X}'$. We call this premise as the *specialized experts condition*.

Since the routing weights $\mathbf{r}(\mathbf{x})$ are convex combinations of the expert attention patterns, the induced attention mapping of MoPE, $\mathcal{A}_{\text{MoPE}}(\mathbf{x}, \mathcal{E}, \mathbf{r})$, is equal to $\text{conv}(\mathcal{E})$:

$$\mathcal{A}_{\text{MoPE}}(\mathbf{x}, \mathcal{E}, \mathbf{r}) = \text{conv}(\mathcal{E}), \quad \forall \mathbf{x} \in \mathcal{X}' \quad (16)$$

Therefore, for each instance $\mathbf{x} \in \mathcal{X}'$, there exists an attention pattern $\mathbf{A}^* \in \mathcal{A}^*(\mathbf{x})$ that is also contained in $\mathcal{A}_{\text{MoPE}}(\mathbf{x}, \mathcal{E}, \mathbf{r}^*)$ for some routing score \mathbf{r}^* , i.e.,

$$\exists \mathbf{A}^* \in \mathcal{A}^*(\mathbf{x}) \cap \mathcal{A}_{\text{MoPE}}(\mathbf{x}, \mathcal{E}, \mathbf{r}^*), \quad \forall \mathbf{x} \in \mathcal{X}' \quad (17)$$

This implies that the attention discrepancy for each instance $\mathbf{x} \in \mathcal{X}'$ under the routing score \mathbf{r}^* is equal to the optimal instance-wise attention discrepancy:

$$\Delta(\mathbf{x}, \mathcal{E}, \mathbf{r}^*) = \inf_{\mathbf{A} \in \mathcal{A}_{\text{MoPE}}(\mathbf{x}, \mathcal{E}, \mathbf{r}^*)} \|\mathbf{A} - \mathbf{A}^*\|_{\mathcal{A}} = \inf_{\mathbf{A} \in \mathcal{A}^*(\mathbf{x})} \|\mathbf{A} - \mathbf{A}^*\|_{\mathcal{A}}, \quad \forall \mathbf{x} \in \mathcal{X}' \quad (18)$$

Therefore, the accumulated attention discrepancy for MoPE under the routing score \mathbf{r}^* across instances in \mathcal{X}' is equal to the sum of the optimal instance-wise attention discrepancies:

$$\sum_{\mathbf{x} \in \mathcal{X}'} \Delta(\mathbf{x}, \mathcal{E}, \mathbf{r}^*) = \sum_{\mathbf{x} \in \mathcal{X}'} \inf_{\mathbf{A} \in \mathcal{A}^*(\mathbf{x})} \|\mathbf{A} - \mathbf{A}^*\|_{\mathcal{A}} \quad (19)$$

which is equivalent as:

$$\sum_{\mathbf{x} \in \mathcal{X}'} \Delta(\mathbf{x}, \mathcal{E}, \mathbf{r}^*) = \sum_{\mathbf{x} \in \mathcal{X}'} \Delta(\mathbf{x}, \mathbf{P}_{\mathbf{x}}^*) \geq 0 \quad (20)$$

Thus, when the number of instances exceeds the number of experts, if the convex hull of the expert attention mappings contains an optimal attention pattern for each instance, then there exists a routing score \mathbf{r}^* that allows MoPE to achieve an accumulated attention discrepancy equal to the sum of the optimal instance-wise attention discrepancies across those instances.

Putting it together, the Theorem 1 state that the global-shared prompt (*i.e.* vanilla prompt) could not achieve the best result, when the input instances require different attention patterns to perform well. Theorem 2 state that it is possible for MoPE to achieve the best result on all of the input instances, conditioned on the appropriate specialization of experts.

B.2 Discussion: How to Choose the Main Modality?

In the proposed method, we use a sequential pipeline to fuse different modalities. In this pipeline, the input of the complementary modality y is first encoded into a representation ψ_y , which is then used to guide the prompting of modality x . This design raises an interesting question: “*How to choose the complementary and main modality?*”

For tasks that do not require a dense representation, such as classification, our experience is that either modality can be used as the main modality, yielding similar results. In our experiments, we utilize vision as the main modality due to empirically better results, but this does not necessarily mean that the text encoder cannot be the main modality. We have also tested using text as the main modality, and the results are summarized in Tab. 6.

As the table shows, using BERT as the main encoder results in a decline in performance. Our postulation is that for these three tasks, the text input

Table 6: Result of Language Model (LM) as main modality.

Method	SNLI-VE	Food-101	MM-IMDB
Ours(LM)	71.10±.12	88.01±.12	58.38±.11/65.81±.23
Ours(VM)	73.59±.15	92.05±.11	62.01±.21/68.24±.12

contains a significant amount of noisy and false positive data. For instance, in the UPMC-Food 101 dataset [41], the text data is derived using a spider, which includes many irrelevant hypertext and website titles. Therefore, treating text as the main modality can lead to overfitting and biased predictions.

For tasks that require a modality-specific dense representation for decoding, such as text generation and segmentation, the main modality must be the one that provides such output. For example, we use the BERT encoder to guide Swin for segmentation, and we use Swin to guide BERT for visual question answering (detail in Appendix C).

B.3 Our MoPE-based method yields a better multimodal representation.

We visualize the multimodal representation generated by different methods using t-SNE. For *LateConcat*, this would be the concatenated feature from both modalities. For the other methods, we visualize the [CLS] token of the main modality. For ease of coloring, we only show the first 20 classes in the test set of the UPMC Food-101 [41] dataset. The results are presented in Fig. 8. As the results show, the representation generated by our method is the most separable.

C Boarder Applications

In this section, we explore the broader applications of our MoPE-based multimodal fusion method beyond classification tasks by providing additional experiments on dense prediction tasks.

C.1 Referring Image Segmentation

The proposed fusion method focuses on utilizing prompts to adapt the Transformer encoders to derive a multimodal representation. Based on this representation, we can tackle tasks beyond classification, such as segmentation. In this section, we briefly introduce how our method can be applied to this scenario and provide experimental results.

Datasets and Task. RefCOCO [13] and RefCOCO+ [13] are the commonly used datasets for referring image segmentation (RIS), both built upon the MSCOCO [24] dataset. RefCOCO contains 142,209 referring expressions for 50,000 objects across 19,994 images, while RefCOCO+ includes 141,564 expressions for 49,856 objects in 19,992 images. The task involves predicting a segmentation

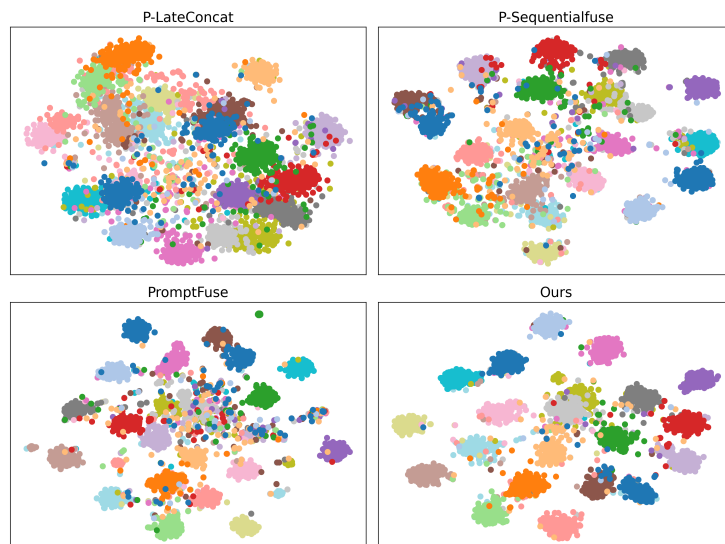


Fig. 8: t-SNE visualization of multimodal representation generated by different methods. The representation generated by our method is the most separable. Better viewed with color.

mask from the input image according to a given referring expression in natural language.

Architecture and Training Details. We utilize ImageNet-pretrained Swin-B-384 as our vision encoder, and we use BERT as the text encoder. For the decoder head, we adopt the standard SETR-PUP [48] head. Following [11], the head is fine-tuned, while we use the MoPE-based tuning method to adapt the encoders. The pyramid feature maps from the 4 Swin layers are fed into the segmentation head for end-to-end training. The optimization uses the same hyperparameters as in our main paper.

Compared Models. To the best of our knowledge, there is no existing prompt-based multimodal fusion method that is compatible with dense visual tasks. Notably, the previous state-of-the-art method, PMF [21], assumes that each encoder uses the same Transformer architecture, and they did not open-source their training code. Furthermore, their prompt tuning is only applied to the deep layers, while SETR-PUP [48] requires pyramid features from internal layers. Therefore, we find it challenging to adapt PMF for dense tasks such as segmentation. Given these challenges, we primarily compare our method with our baselines, *SequentialFuse* and *p-SequentialFuse*.

Quantitative Comparison with Baselines. The quantitative results, measured as mean Intersection over Union (mIoU) on the validation and test sets of RefCOCO and RefCOCO+, are reported in Tab. 7. As shown in the table, our MoPE-based method achieves the best performance. We outperform the prompt-based method, *p-SequentialFuse*, by a significant margin. Additionally,

our method performs better than the fine-tuning method. We observe that the fine-tuning method tends to overfit in this experimental setting.

Table 7: Segmentation results on RefCOCO and RefCOCO+. We report the total number of parameters in million (including the trainable segmentation head), and metrics (mIOU) on RefCOCO and RefCOCO+.

Method	Param	RefCOCO(↑)			RefCOCO+(↑)		
		val	testA	testB	val	testA	testB
SequentialFuse	231.0M	53.48	55.76	52.03	40.22	42.2	37.91
P-SequentialFuse	35.1M	47.69	46.23	45.81	30.66	31.48	28.79
Ours	35.5M	58.40	60.03	53.23	43.80	46.12	38.88

Visualization of segmentation result. We visualize the segmentation results in Figures 9 and 10. As the results show, our MoPE-based segmentation method can better locate the object according to the referring image segmentation task. In contrast, the method based on global-shared prompts, p-SequentialFuse, may struggle to understand the text instructions and provide incorrect results.

C.2 Additional Examples of Expert Routing on VQAv2

Our MoPE is designed to scale up the expressiveness of vanilla prompts, and expert specialization is a critical condition to achieve superior results as well as interpretability. To further demonstrate expert specialization, we train our MoPE-based method on an even larger dataset, VQAv2 [8]. This dataset contains 265,016 images and paired questions, covering a wide array of visual and textual concepts. We train our model on this dataset and visualize the routing results in Figures 11, 12, 13, and 14. We observe clear expert specialization in these examples, where different experts capture different concepts.

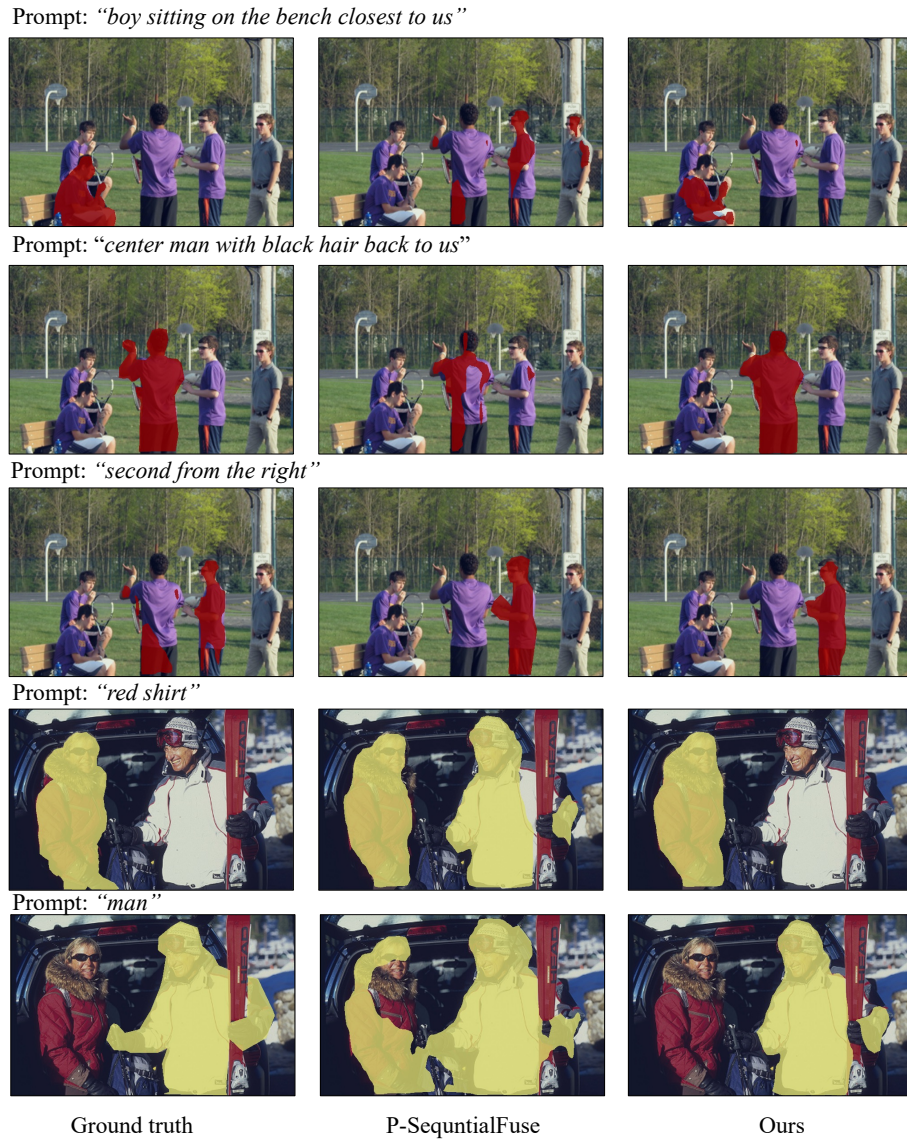


Fig. 9: Quantitative result of referring image segmentation. Better viewed with color.



Fig. 10: Quantitative result of referring image segmentation (cont). Better viewed with color.



Fig. 11: Additional example of expert routing - 1. We show routing result of expert-4 on VQAv2 dataset, which specialize in animals. Note: Sorted by routing score, images and texts may not in same order.



Fig. 12: Additional example of expert routing - 2. We show routing result of expert-6 on VQAv2 dataset, which specialize in lighting conditions. Note: Sorted by routing score, images and texts may not in same order.



Fig. 13: Additional example of expert routing - 3. We show routing result of expert-8 on VQAv2 dataset, which specialize in toilet-related concepts and hairstyles. Note: Sorted by routing score, images and texts may not in same order.



Fig. 14: Additional example of expert routing - 4. We show routing result of expert-10 on VQAv2 dataset, which specialize in weather conditions. Note: Sorted by routing score, images and texts may not in same order.